The multiple roles of an organic corrosion inhibitor on copper investigated by a combination of electrochemistry-coupled optical in situ spectroscopies

Ying-Hsuan Chen[a], Andreas Erbe[a,b,*]

[a] *Max-Planck-Institut für Eisenforschung GmbH, Max-Planck-Str. 1, 40237 Düsseldorf, Germany.*
[b] *Department of Materials Science and Engineering, NTNU, Norwegian University of Science and Technology, 7491 Trondheim, Norway.*

Abstract

The interaction of the organic corrosion inhibitor 2-mercaptobenzothiazole (MBT) with copper in alkaline solution was investigated by in situ infrared (IR) and Raman spectroscopy, and in situ spectroscopic ellipsometry, coupled to cyclic voltammetry (CV). At negative potentials, MBT monolayers relax on a minute time scale through MBT reorientation, leading to MBT-copper binding via S and N-atoms. After copper dissolution becomes thermodynamically feasible, including at open circuit, formation of a multilayer CuMBT complex sets in, in which thiol dominates over thione. Multilayer films effectively inhibit oxide formation. Instead, MBT oxidatively dimerises to 2,2'-dibenzothiazole disulfide (DBTA), which remains protective.

Keywords: A. copper, B. cyclic voltammetry, B. ellipsometry, B. IR spectroscopy, B. Raman spectroscopy, C. alkaline corrosion

1. Introduction

The use of corrosion inhibitors an efficient and effective ways to prevent metal corrosion [1–3]. Many low molecular weight organic compounds form a protective layer on the metal surface to block the access of oxidants, water

*Corresponding author
Email address: MBT-on-Cu@the-passivists.org (Andreas Erbe)

or ions to the metal surface, and slow down corrosion [4–6]. The presence of heteroatoms in organic compounds usually promotes the compound's adsorption to a metal surface, hence facilitating effective corrosion inhibition [5, 7–10].

Benzotriazole (BTA) and its thiolated form 2-mercaptobenzothiazole (MBT) are well known organic corrosion inhibitors, amongst others, for copper [1, 11]. Both BTA and MBT can react with copper ions to form a copper complex film covering the metal surface [12–14]. Some studies show MBT to have a higher inhibition efficiency than BTA [15, 16]. However, compared to BTA [17, 18], there were only few studies focusing on MBT. MBT exists in both a thiol and a thione form, and has been found an effective corrosion inhibitor also to zinc [19, 20].

To data, most available studies on the interaction of copper with MBT have used surface modification and ex situ analysis after transfer of the sample through an oxygen containing atmosphere [21–23]. Ex situ x-ray photoelectron spectroscopy (XPS) after sample transfer through air has been widely used to understand the nature of the MBT layer forming on Cu. Kazansky et al. [20, 21, 24] suggest that a thin Cu_2O layer on Cu surface was required for the formation of a CuMBT film. The forming CuMBT layer became thicker if Cu was immersed longer in MBT solution. Studies from Finšgar et al. [23] showed by angle dependent XPS that the MBT nitrogen and exocyclic sulfur atom were involved in MBT adsorption to Cu. Moreover, no Cu^{2+} species were detected, neither in the CuMBT complex layer, nor on the Cu surface after Cu was treated with MBT. This observation implies that the CuMBT complex contains Cu^{+}. Potentiodynamic electrochemical experiments showed MBT to act as a mixed-type inhibitor, i.e. inhibiting both cathodic and anodic processes on the surface [23].

Other surface analysis techniques were also applied to investigate the behavior of MBT in different solutions [11, 25–29]. Non-destructive in situ spectroscopies are also introduced in this field. Woods et al. [30] used surface enhanced Raman spectroscopy (SERS) to investigate the interaction of MBT with Cu, Ag and Au. In situ SERS was recorded for Cu at controlled electrode poten-

tial in solutions containing MBT at different pH. It was shown that oxidative charge transfer adsorption of MBT on the copper surface occurred in alkaline solution; while in acid medium, the charge transfer occurred only at higher electrode potential. The spectra also revealed that MBT interacted with Cu in the thiol form. Huo et al. [22] obtained similar results. The interaction between MBT and Cu was investigated in 0.1 M $NaClO_4$ using electrochemical surface-enhanced infrared (IR) spectroscopy in attenuated total reflection (ATR) mode. It was found that at lower potential, MBT vertically adsorbed on the Cu surface in the form of a thiolate, while at higher potential nitrogen atom and exocyclic sulfur atom coordinates to Cu^+ to form complex polymer on the surface [22]. All previous in situ studies focus on the application of a single technique. No detailed in situ studies are available allowing to disentangle the role of inhibitor adsorption, metal dissolution, and oxide formation. In particular, the competition between oxide film formation and inhibitor film formation has not been investigated in situ.

In this work, three different complementary in situ spectroscopic techniques were applied to study the interaction of MBT with Cu in 1 mM MBT alkaline solution. In situ surface enhanced ATR-IR and in situ Raman spectroscopy were used to investigate the CuMBT complex molecular structure, as well as oxide formation on the surface. In situ spectroscopic ellipsometry was used to determine the thickness of the interfacial layer. Both Raman and ellipsometry experiments were conducted during cyclic voltammetry (CV), while IR spectroscopy was conducted at open circuit potential (OCP). This combination of several in situ techniques promises more detailed insight into the potential dependence of the interfacial structure of copper in contact with an MBT-containing electrolyte.

2. Materials and methods

2.1. Sample preparation

For in situ IR spectroscopic experiments, a Cu layer was used which was chemically deposited on a Ge(100) single crystal wafer. This copper sample was later used as substrate for MBT adsorption. Based on an established recipe [31], 0.2547 g $CuSO_4 \cdot H_2O$ (Sigma-Aldrich), 1.2579 g potassium sodium tartrate, $C_4H_4O_6KNa \cdot 4H_2O$ (Sigma-Aldrich) and 0.4318 g NaOH (Merck) were dissolved in 50 mL ultrapure water. After all the solid was dissolved, 1 mL formaldehyde, HCHO, (Sigma-Aldrich) was added into the solution. The pH was adjusted to 13 with concentrated HCl to give a clear blue solution. To prepare the chemically deposited Cu layer on the ATR Ge crystal, the double side polished Ge(100) crystal (0.5 mm; Crystal GmbH) was cut into a size of 52 mm·20 mm, and both shorter sides were polished to an angle of 30° to be used for ATR measurement at 60° angle of incidence [32]. The crystal was cleaned by washing with isopropanol and ultrapure water. The copper layer was prepared by dropping the solution prepared as described above on the germanium layer such that it covers the area to be sampled subsequently. The solution was left on the germanium for 5 min to give a deposited Cu layer. Finally, the blue deposition solution was removed from the crystal by washing with ultrapure water, and the freshly prepares surface was used for subsequent experiments.

For in situ Raman and spectroscopic ellipsometry experiments, evaporated Cu on a Si(100) wafers was used. Si(100) wafers (Siegert Wafer) were washed with isopropanol and ultrapure water. First, a 10 nm titanium adhesion layer was e-beam evaporated. Then a 200 nm copper layer was deposited, with the evaporation rate of 1 Å/s. For electrochemical measurements, 0.1 M aqueous NaOH was prepared from NaOH (Merck) and ultrapure water. In the 0.1 M NaOH, a 1 mM solution of MBT (Sigma-Aldrich) was prepared.

2.2. In situ IR spectroscopy

The home-built three electrode electrochemical cell [32, 33] with electrode area of 4 cm^2 was placed into a sample chamber of a Bruker Vertex 70v Fourier

transform IR spectrometer (Bruker Optik GmbH, Ettlingen, Germany). The spectrometer was equipped with a middle band mercury cadmium telluride (MCT) detector which was cooled with liquid nitrogen for 1 h before measurements. All IR spectra were accumulating 100 scans with a spectral resolution of 4 cm^{-1}. For time-dependent measurement, p-polarized light was used. The reference spectrum was taken ≈5 min after MBT in NaOH was was introduced into the cell under open circuit conditions. Afterwards, spectra were continuously recorded.

2.3. In situ Raman spectroscopy

Raman spectra were recorded on a Labram confocal Raman microscope (Horiba Jobin Yvon), with an excitation wavelength of 632 nm of a HeNe laser. An objective with magnification 10× and numerical aperture 0.25 was used to illuminate the sample with an illuminated spot with 10 μm diameter. The resulting spectra were analysed on a CCD detector. For monitoring electrochemical processes, a home-built three electrode electrochemical cell was used, with electrode area of 0.785 cm^2 [34, 35]. Electrode potential was controlled by a potentiostat (Palmsens). The Raman spectra were recorded with an integration time of ≈32 s.

2.4. In situ spectroscopic ellipsometry

Spectroscopic ellipsometry measurements were performed using an SE800 UV/Vis spectroscopic ellipsometer (Sentech Instruments), with a xenon source, in the wavelength range of 300−820 nm, at an angle of incidence of 70°. Concurrent electrochemical experiments were conducted in a home-built three electrode electrochemical cell with electrode area of 2.5 cm^2. The illuminated area on the working electrode was 0.7 cm^2 [36, 37]. Electrode potential was controlled by a Compactstat potentiostat (Ivium Technologies). Recording one ellipsometric spectrum required ≈35 s. The thickness of CuMBT film was analysed by a method described previously [38], using calculated values of differences in the ellipsometric parameter Δ averaged over a wavelength range from 700 nm to

750 nm for a given thickness as calibration. It was assumed that refractive index of copper oxides roughly equals the one of the CuMBT complex. No data was available for the refractive index of CuMBT. As transition metal complex, it is likely to be higher than the refractive index of pure MBT, which was reported as 1.785 [39]. Uncertainties were estimated via Gaussian uncertainty propagation; the standard deviation of the ellipsometric parameter Δ was estimated in a region at low potential when it was expected to be stable, and used to estimate the standard deviation of the thickness. Uncertainties are reported as single standard deviation.

2.5. Electrochemical experiments

Electrode potential E is reported with reference to Ag|AgCl|3 M KCl. Current was normalized to electrode area and is reported as current density j. An Ag|AgCl|3 M KCl microreference electrode (World Precision Instruments) was used. A graphite rod was used as counter electrode in Raman spectroscopy measurements, while a Pt mesh was used in IR and spectroscopic ellipsometry measurements. Before experiments started, all the solutions were purged with Argon for at least 30 min.

For time dependent in situ IR measurements, chemically deposited copper (section 2.1) was used as working electrode. After preparation, the surface was immediately used for experiments. The 1 mM MBT solution in 0.1 M NaOH was directly introduced into the cell.

For potential dependent in situ Raman and spectroscopic ellipsometry experiments, evaporated Cu was used. First, a potential of -1.0 V in 0.1 M NaOH was applied for 10 min to reduce the oxide. Reference experiments on pure Cu in pure 0.1 M NaOH were performed. In order to compare how oxidation would be affected by MBT, after the surface was reduced, 1 mM MBT in NaOH was introduced into a cell by a flow system, while the electrode potential was kept at -1.0 V for 30 min. A cyclic voltammogram (CV) was recorded in both reference and MBT experiments, from -1.0 V to 0.5 V, with starting electrode potential -1.0 V and scan rate 1 mV/s.

3. Result and discussion

3.1. In situ IR experiments

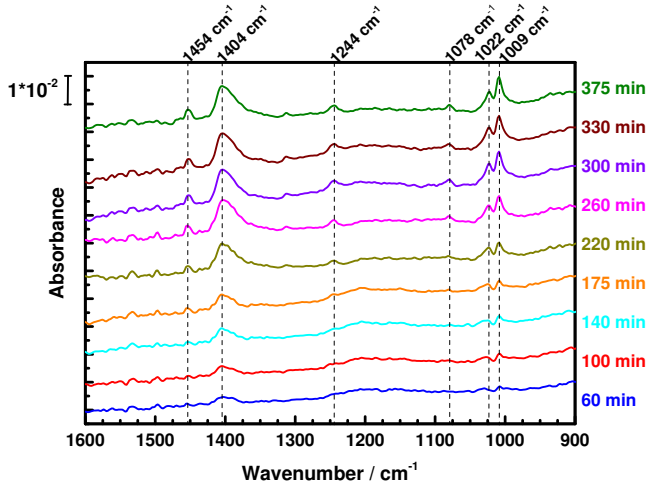

Figure 1: Time-dependent IR spectra recorded in 1 mM MBT / 0.1M NaOH. Spectra have been vertically offset for clarity.

Time-lapse IR spectra at open circuit explored the interaction between Cu and MBT (Fig. 1). As immersion time increased, four peaks at 1009 cm^{-1}, 1022 cm^{-1}, 1244 cm^{-1} and 1404 cm^{-1} appeared. These peaks were assigned to C−S thiol stretching, C=S thione stretching, C−N stretching in the NCS ring and NCS ring stretching, respectively, of CuMBT complexes [22, 40]. The increase in absorbance indicates a progressive formation of CuMBT complexes. The absorbance increase of the peaks at 1009 cm^{-1} and 1022 cm^{-1} did not proceed in the same manner. Initially, both peaks had approximately the same absorbance, however, in the course of the experiment, the 1009 cm^{-1} peak significantly gained in absorbance. At the end, absorbance at 1009 cm^{-1}, characteristic for the thiol form, was higher than at 1022 cm^{-1}, characteristic for the thione form [22, 40]. Based on this observation, we infer that the thiol form is dominant in the formed CuMBT complex.

3.2. *In situ Raman spectra and ellipsometry*

3.2.1. *Formation of a CuMBT film*

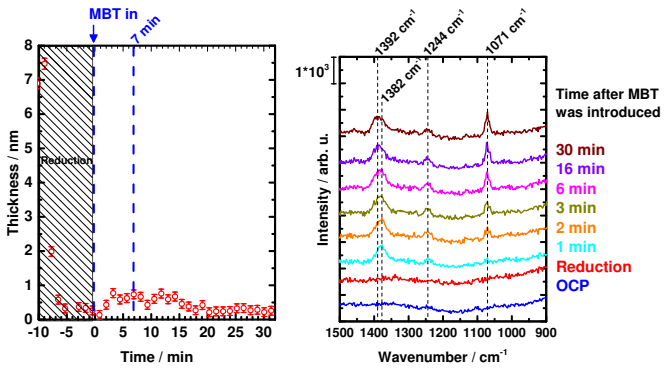

(a) (b)

Figure 2: (a) Thickness of interfacial layer from ellipsometry, and (b) time dependent in situ Raman spectra for Cu in 1 mM MBT / 0.1 M NaOH at -1.0 V. In (a) the electrode potential was kept at -1.0 V during the whole process. The injection of MBT started at time 0. (b) The spectrum at OCP was collected before reduction. The spectrum labelled "Reduction" was recorded before introducing MBT. Times refer to the time after injection of MBT.

Ellipsometric data in Fig. 2(a) shows a rapid decrease in thickness after reduction started, because of a reduction of copper oxide. After ≈10 min, MBT was introduced into the cell, and an increase of thickness to 1.5 nm was observed, indicating a growth of a CuMBT complex film on the Cu surface. Thickness stopped to increase ≈5 min after introduction of MBT, and started to decrease, implying a structural change at the metal/solution interface. The thickness continued decreasing as time increased, and thickness reached ≈0.5 nm after ≈30 min.

Fig. 2(b) shows the related in situ Raman spectra. Immediately after MBT addition, two peaks at 1244 cm^{-1} and 1382 cm^{-1} were observed, both of which were assigned to CuMBT complex NCS ring stretching [30, 40], indicating the formation of a CuMBT film. At the second minute, a peak at 1071 cm^{-1} started to be observed. This peak was assigned to an asymmetric stretching of both benzene and NCS ring [30, 40]. As time increased, the intensity of the peaks at

1244 cm^{-1} and 1382 cm^{-1} didn't change significantly. Nevertheless, the peak at 1071 cm^{-1} grew with time.

We propose a reorientation as cause of the intensity increase of the peak at 1071 cm^{-1} here, which does at the same time lead to the observed decrease in layer thickness. MBT molecules are proposed to adsorb initially on the Cu surface vertically with the exo-S atom (Fig. 3). In later stages, as precursor for the formation of a CuMBT complex film, MBT changes its orientation as illustrated (Fig. 3), such that both N and exo-S atoms were in contact with the Cu surface. Such an interpretation is in agreement to the structure reported from ex situ XP spectra, where N and exo-S atoms were involved in the formation of the CuMBT complex [23]. This reorientation leads to the decrease of interfacial thickness at constant potential. Molecular dimensions of MBT were reported as length of ≈0.70 nm and width of 0.50 nm [41, 42]. It agreed with our observation of interfacial thickness, which was initially 1.5 nm and reached 0.5 nm at the end. In addition, we observed a shift of the peak initially at 1382 cm^{-1} to 1392 cm^{-1}. In ex situ data, this peak of a synthesized CuMBT complex in solid state was found at 1405 cm^{-1} [30]. This Raman shift was found to be affected by the Cu surface [30]. If MBT is adsorbed to the surface, the electron density of its heterocyclic ring would be reduced due to the comparatively electron deficient Cu surface, leading to the reduction of the double bond character of the NCS ring, and resulting in a shift to lower wavenumber of the NCS ring stretching peak [30]. In their case [30], a peak at 1394 cm^{-1}, proposed from surface CuMBT complex, was detected in buffer solution of pH 9.2 at +0.1 V. The shift in the aforementioned Raman peak with time therefore indicates a change in the interaction between the copper surface and MBT changes, further supporting our hypothesis of reorientation. This red shift can be attributed to the influence of Cu surface. Bound to a Cu surface, the electron density in the MBT ring would reduce due to the attraction of comparatively electron-deficient Cu atoms [30]. Therefore, it led to the reduction of the double bond character of NCS ring, and resulted in the shift to lower wavenumber of NCS ring stretching peak [30].

The interfacial thickness indicates that only a monolayer film formed on the

surface, and this film didn't grow with time. Unlike in situ IR spectroscopy which was monitored at open circuit potential, Raman and ellipsometry measurement were performed at -1.0 V; this electrode potential was too low to produce more Cu ions to permit multilayer formation of CuMBT complexes. In previous studies, based on post mortem analysis, formation of a Cu_2O layer on Cu was suggested to be crucial to the subsequent formation of CuMBT complexes [20, 21, 24]. In this case, we expect most of the oxide to be removed after 10 min polarization at -1.0 V. Moreover, there was no Cu_2O related peak detected in the in situ Raman spectra. Consequently, from the in situ data gathered here, there is no evidence that Cu_2O is essential for CuMBT complex formation. However, it is still possible that fractions of the oxide was not removed, and was not detected in Raman spectra.

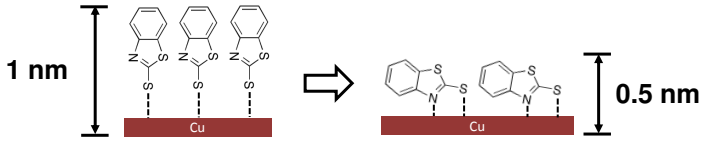

Figure 3: Proposed mechanism of MBT adsorption on Cu under reducing conditions in NaOH.

3.2.2. Inhibition of oxide formation

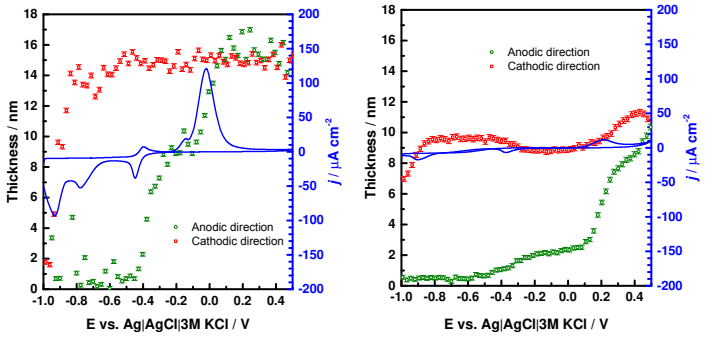

(a) (b)

Figure 4: Current density and thickness of interfacial layer as function of applied electrode potential, (a) in 0.1 M NaOH (b) in 1 mM MBT/0.1 M NaOH.

Oxide formation on Cu in the absence of MBT was initially investigated. Fig. 4(a) shows the CV and corresponding thickness change obtained from analysing ellipsometric spectra. In the CV, three anodic peaks and three cathodic peaks were observed. The anodic peaks at -0.4 V and 0.0 V were attributed to the formation of Cu_2O and CuO, respectively [43, 44]. During the anodic reactions, two setps with increase of thickness were observed. The first thickness increase started at -0.4 V, and reached 9 nm at -0.2 V. The second increase started at -0.1 V, and reached 16 nm at +0.1 V. Above +0.1 V, there was no obvious thickness increase, and the thickness remained at ≈16 nm. The two stages of increase agreed in potential to anodic peaks observed in the CV. In the cathodic reaction, the cathodic peaks at -0.4 V and -0.9 V were assigned to the reduction of Cu_2O and CuO, respectively. However, there was no obvious decrease in thickness at -0.4 V. As the electrode potential reached -0.8 V that the thickness started to decrease, and it reached 2 nm at -1.0 V. Surface roughening may lead to an apparent thickness larger than 0.

Fig. 4(b) shows the corresponding experiment in the presence of MBT. Compared with the NaOH case, both peak current density and thickness were significantly lower, showing that Cu oxidation was effectively inhibited by the presence of MBT. The CV showed only one anodic peak, while three cathodic peaks were detected. The initial thickness was 0.5 nm, which can be attributed to the formation of a CuMBT surface layer. As electrode potential increased, the thickness increased. Layer thickness also increased in two stages, smeared out over a large potential range. The first stage started at -0.6 V, and reached 3 nm at +0.2 V. The second stage started at +0.2 V and reached 8 nm at the end of the anodic process. The thickness continued to increase until +0.4 V after reversing the scan direction before it started to decrease.

In Raman spectra in the absence of MBT [Fig. 5(a)], at -1.0 V, only the water peak at 1640 cm^{-1} was observed. When the electrode potential reached 0.0 V in the experiments increasing potential, a peak at 523 cm^{-1} appeared, which was assigned to the A_{1g} mode of Cu_4O_3 [45, 46], implying the formation of copper oxide [34]. The appearance of this peak was consistent with the

thickness increase observed at 0.0 V. However, at -0.4 V, the position of the first anodic peak, there was no obvious change in spectra. We didn't observe CuO and Cu_2O related peaks in any Raman spectra. It is possible that amorphous oxide was formed, so that the peaks were too broad to be observed. With increasing electrode potential, both water and Cu_4O_3 peaks decreased. The decrease of water peak can be attributed to oxide formation on the surface. The decrease of Cu_4O_3 peak is interpreted as transformation of Cu_4O_3 to other copper oxides, presumably CuO, at higher electrode potential. (Alternatively, soluble Cu^{2+} species may also form [47].) During the negative scan, the peak at 523 cm^{-1} increased, implying the reformation of Cu_4O_3. A very strong increase at 700 cm^{-1} was observed when the electrode potential reached -0.8 V. Peaks in this range have been assigned to Cu−OH species formed after reduction [43].

Fig. 5(c) shows in situ Raman spectra in the presence of MBT. At -1.0 V, the peaks at 1071 cm^{-1}, 1244 cm^{-1} and 1392 cm^{-1} were observed, related to CuMBT complex formation. As electrode potential increased, the latter peak shifted to 1400 cm^{-1}, which it reached at -0.2 V. A peak wavenumber of 1405 cm^{-1} was obtained for bulk CuMBT [30]. Observations here indicate possible differences between surface species and bulk species of CuMBT. As discussed in section 3.2.1, this red shift can be attributed to the influence of the copper surface. Bound to a copper surface, the electron density in the MBT ring would reduce due to the attraction of comparatively electron-deficient Cu atoms [30]. Therefore, it led to the reduction of the double bond character of NCS ring, and resulted in the red shift of NCS ring stretching peak [30]. Peak shift also indicated the formation of a multilayer. Top layers were less affected by the Cu surface, so the positions of peak is closer to bulk CuMBT [30]. Peak shift for multilayer formation is significantly larger than during reorientation of the molecules in the monolayer discussed in section 3.2.1.

When the electrode potential reached +0.2 V, peaks at 501 cm^{-1}, 1010 cm^{-1}, 1126 cm^{-1}, 1238 cm^{-1}, 1276 cm^{-1}, 1425 cm^{-1} and 1463 cm^{-1} started appear in the spectra. These peaks indicate the presence of 2,2'-dibenzothiazole disulfide (DBTA), an disulfide dimer of MBT resulting from its partial oxidation [30].

As electrode potential increased, the intensity of DBTA-related peaks increased, indicating increased amount of DBTA on the surface. At the same time, the amount of CuMBT did not change, since there was no obvious change in intensity. When scanning in negative direction [Fig. 5(d)], the intensity of DBTA related peaks continued increasing until +0.2 V was reached, then started to decrease until -1.0 V, where no DBTA was observed any longer. The peaks originating from CuMBT decreased slightly from +0.4 V to -0.4 V. When -0.6 V was reached, the peak at 1400 cm^{-1} shifted back to 1392 cm^{-1}, implying only the surface CuMBT species remained, and the bulk complex in the multilayers on top was removed. However, compared with the spectra recorded at the initial -1.0 V, the intensity was higher after one cycle. Consequently, after electrode potential sweeping, the surface species changed. Comparing these spectra with those measured in NaOH shows the absence of a copper oxide related peak at $\approx$523 cm^{-1}. The effective inhibition of copper oxide formation was proven.

The observed two stage layer thickness increase in the ellipsometric CV in the presence of MBT [Fig. 4(b)] can hence be excluded to originate from copper oxide formation: neither was there an anodic peak in the CV, nor were copper oxide peaks observed in Raman spectra. The first stage with increasing layer thickness can be attributed to continuous formation of a CuMBT complex. The second stage can be attributed to the formation of DBTA in the surface layer. DBTA formation also manifests in the anodic peak at +0.2 V, indicating the oxidation of MBT molecules.

After reversing scan direction, thickness kept increasing until the potential returned to +0.4 V. Subsequently, thickness decreased until 0.0 V. According to in situ Raman spectra, this decrease was due to the reduction of DBTA. However, there was no cathodic peak observed here. Therefore, the decrease in layer thickness either resulted from depletion, or from a localised molecular electron transfer. Electrochemical reduction of DBTA can be excluded. From 0.0 V to -0.35 V, the thickness remained constant. At $\approx$-0.35 V, there was a slight increase in thickness, together with appearance of a cathodic peak. We argue that this behaviour may be related to a shift at -0.6 V in Raman spectra,

a change of the CuMBT complex layer. At -0.85 V, there was a large decrease in thickness and a corresponding cathodic peak appeared at -0.9 V. This decrease can be attributed to the electrochemical reduction of DBTA, since the related peaks can be hardly observed at -1.0 V in Raman spectra.

4. Conclusion

MBT adsorbs in a monolayer at reducing conditions at the oxide-free Cu surface in alkaline electrolyte, as show by in situ ellipsometry and Raman spectroscopy. At constant electrode potential, the film undergoes a relaxation with an orientation change of the MBT molecules. At larger potentials and also under open circuit conditions, a copper MBT complex multilayer film forms. In this film, the thiol form of MBT dominates over thione form. After formation of the film, it effectively inhibits oxide formation. At positive potentials, formation of the disulfide oxidation product of MBT prevents surface oxidation. Overall, this study shows the quite complex role of the molecular corrosion inhibitor, and lets one reflect on design criteria for molecular corrosion inhibitors: they need to form stable but dynamic bounds to the metal surface to be protected via multiple binding sites, they need to be able to form complexes with oxidation products of the metal, and their own oxidation products need to contribute to upholding surface protection. In that manner, MBT acts as a "sacrificial inhibitor"; oxidation of the inhibitor molecule happens instead of oxidation of the metal surface.

Acknowledgments

Cigdem Toparli, Petra Ebbinghaus and Martin Rabe are acknowledged for technical assistance and fruitful discussions. Y.H.C. thanks the German Academic Exchange Service (DAAD) for a scholarship. A.E. thanks Prof. M. Stratmann for continuous support.

Data statement

Research data collected by the different in situ spectroscopy methods will be made available as soon as publication of the manuscript is foreseeable via the Max Planck Societies open access data repository Edmond, `http://edmond.mpdl.mpg.de/`.

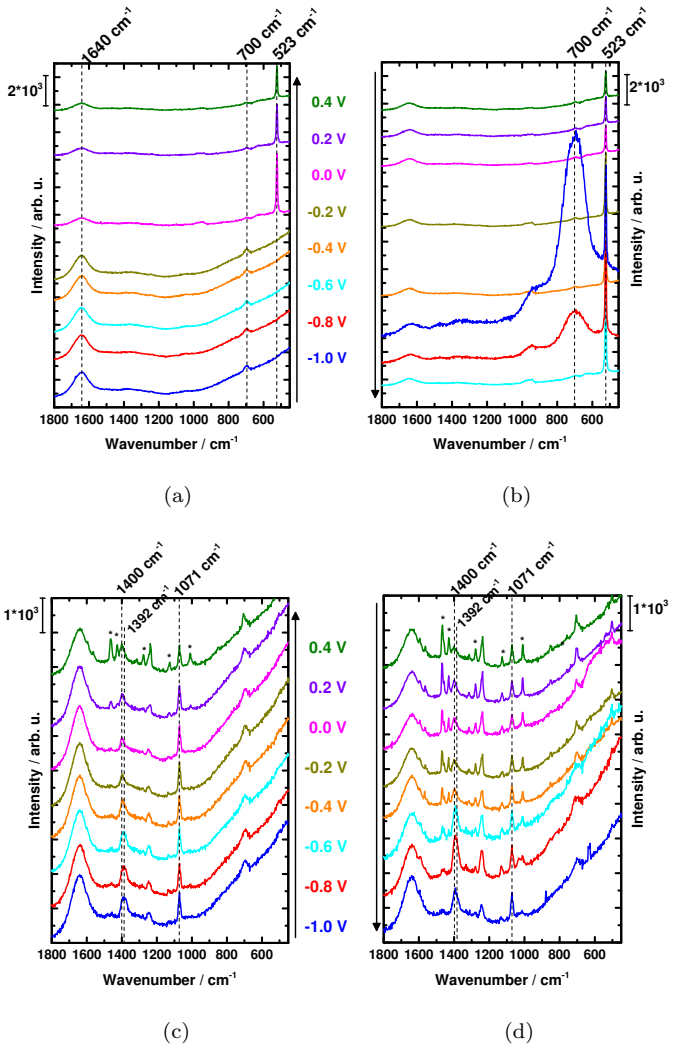

Figure 5: Raman spectra recorded during CV for Cu in 0.1 M NaOH during (a) positive and (b) negative potential direction; in 1 mM MBT / 0.1 M NaOH during (c) positive and (d) negative potential direction.

References

[1] M. M. Antonijevic, M. B. Petrovic, Copper corrosion inhibitors. A review, Int. J. Electrochem. Sci. 3 (2008) 1–28.

[2] M. Finšgar, J. Jackson, Application of corrosion inhibitors for steels in acidic media for the oil and gas industry: A review, Corros. Sci. 86 (2014) 17 – 41. doi:http://dx.doi.org/10.1016/j.corsci.2014.04.044.
URL http://www.sciencedirect.com/science/article/pii/S0010938X14002157

[3] P. B. Raja, M. Ismail, S. Ghoreishiamiri, J. Mirza, M. C. Ismail, S. Kakooei, A. A. Rahim, Reviews on corrosion inhibitors: A short view, Chem. Eng. Commun. 203 (9) (2016) 1145–1156. arXiv:http://dx.doi.org/10.1080/00986445.2016.1172485, doi:10.1080/00986445.2016.1172485.
URL http://dx.doi.org/10.1080/00986445.2016.1172485

[4] M. M. Antonijević, S. M. Milić, M. B. Petrović, Films formed on copper surface in chloride media in the presence of azoles, Corros. Sci. 51 (6) (2009) 1228 – 1237. doi:http://dx.doi.org/10.1016/j.corsci.2009.03.026.
URL http://www.sciencedirect.com/science/article/pii/S0010938X09001322

[5] J. Izquierdo, J. J. Santana, S. González, R. M. Souto, Scanning microelectrochemical characterization of the anti-corrosion performance of inhibitor films formed by 2-mercaptobenzimidazole on copper, Prog. Org. Coat. 74 (3) (2012) 526 – 533. doi:http://dx.doi.org/10.1016/j.porgcoat.2012.01.019.
URL http://www.sciencedirect.com/science/article/pii/S0300944012000355

[6] B. Duran, G. Bereket, M. Duran, Electrochemical synthesis and characterization of poly(m-phenylenediamine) films on copper for corrosion protection, Prog. Org. Coat. 73 (2) (2012) 162 – 168.

doi:http://dx.doi.org/10.1016/j.porgcoat.2011.10.008.
URL http://www.sciencedirect.com/science/article/pii/S0300944011003092

[7] C. Yan, H. Lin, C. Cao, Investigation of inhibition of 2-mercaptobenzoxazole for copper corrosion, Electrochim. Acta 45 (17) (2000) 2815 – 2821. doi:http://dx.doi.org/10.1016/S0013-4686(00)00385-6.
URL http://www.sciencedirect.com/science/article/pii/S0013468600003856

[8] T. Shahrabi, H. Tavakholi, M. Hosseini, Corrosion inhibition of copper in sulphuric acid by some nitrogen heterocyclic compounds, Anti-Corros. Methods Mater. 54 (5) (2007) 308–313. arXiv:https://doi.org/10.1108/00035590710822161, doi:10.1108/00035590710822161.
URL https://doi.org/10.1108/00035590710822161

[9] A. Zarrouk, B. Hammouti, A. Dafali, H. Zarrok, R. Touzani, M. Bouachrine, M. Zertoubi, Inhibition of copper corrosion in acid solution by N-1-naphthylethylenediamine dihydrochloride monomethanolate: experimental and theoretical study: part-1, Res. Chem. Intermed. 38 (3) (2012) 1079–1089. doi:10.1007/s11164-011-0444-2.
URL https://doi.org/10.1007/s11164-011-0444-2

[10] A. Zarrouk, B. Hammouti, H. Zarrok, S. S. Al-Deyab, I. Warad, Thermodynamic study of metal corrosion and inhibitor adsorption processes in copper/N-1-naphthylethylenediamine dihydrochloride monomethanolate/nitric acid system: part 2, Res. Chem. Intermed. 38 (7) (2012) 1655–1668. doi:10.1007/s11164-012-0492-2.
URL https://doi.org/10.1007/s11164-012-0492-2

[11] M. L. Lewis, K. T. Carron, Surface-enhanced Raman spectroscopy as a method for determining surface structures, in: M. W. Urban,

C. D. Craver (Eds.), Structure-Property Relations in Polymers, American Chemical Society, Wahington, DC, USA, 1993, Ch. 14, pp. 377–391. arXiv:http://pubs.acs.org/doi/pdf/10.1021/ba-1993-0236.ch014, doi:10.1021/ba-1993-0236.ch014.
URL http://pubs.acs.org/doi/abs/10.1021/ba-1993-0236.ch014

[12] X. Ye, X. Xin, J. Zhu, Z. Xue, Coordination compound films of 1-phenyl-5-mercaptotetrazole on copper surface, Appl. Surf. Sci. 135 (1) (1998) 307 – 317. doi:http://dx.doi.org/10.1016/S0169-4332(98)00301-8.
URL http://www.sciencedirect.com/science/article/pii/S0169433298003018

[13] Y. S. Tan, M. P. Srinivasan, S. O. Pehkonen, S. Y. M. Chooi, Self-assembled organic thin films on electroplated copper for prevention of corrosion, J. Vac. Sci. Technol. A 22 (4) (2004) 1917–1925. arXiv:http://dx.doi.org/10.1116/1.1763901, doi:10.1116/1.1763901.
URL http://dx.doi.org/10.1116/1.1763901

[14] M. Serdechnova, A. N. Salak, F. S. Barbosa, D. E. Vieira, J. Tedim, M. L. Zheludkevich, M. G. Ferreira, Interlayer intercalation and arrangement of 2-mercaptobenzothiazolate and 1,2,3-benzotriazolate anions in layered double hydroxides: In situ x-ray diffraction study, J. Solid State Chem. 233 (2016) 158 – 165. doi:https://doi.org/10.1016/j.jssc.2015.10.023.
URL http://www.sciencedirect.com/science/article/pii/S0022459615302127

[15] R. Subramanian, V. Lakshminarayanan, Effect of adsorption of some azoles on copper passivation in alkaline medium, Corros. Sci. 44 (3) (2002) 535 – 554. doi:http://dx.doi.org/10.1016/S0010-938X(01)00085-3.
URL http://www.sciencedirect.com/science/article/pii/S0010938X01000853

[16] F. Altaf, R. Qureshi, S. Ahmed, Surface protection of copper by azoles in borate buffers-voltammetric and impedance analy-

sis, J. Electroanal. Chem. 659 (2) (2011) 134 – 142. doi:http://dx.doi.org/10.1016/j.jelechem.2011.05.013.
URL http://www.sciencedirect.com/science/article/pii/S157266571100258X

[17] N. K. Allam, A. A. Nazeer, E. A. Ashour, A review of the effects of benzotriazole on the corrosion of copper and copper alloys in clean and polluted environments, J. Appl. Electrochem. 39 (7) (2009) 961–969. doi:10.1007/s10800-009-9779-4.
URL https://doi.org/10.1007/s10800-009-9779-4

[18] M. Finšgar, I. Milošev, Inhibition of copper corrosion by 1,2,3-benzotriazole: A review, Corros. Sci. 52 (9) (2010) 2737 – 2749. doi:http://dx.doi.org/10.1016/j.corsci.2010.05.002.
URL http://www.sciencedirect.com/science/article/pii/S0010938X10002283

[19] H. Yang, Y. Sun, J. Ji, W. Song, X. Zhu, Y. Yao, Z. Zhang, 2-mercaptobenzothiazole monolayers on zinc and silver surfaces for anticorrosion, Corros. Sci. 50 (11) (2008) 3160 – 3167. doi:http://dx.doi.org/10.1016/j.corsci.2008.08.036.
URL http://www.sciencedirect.com/science/article/pii/S0010938X08003417

[20] I. A. Arkhipushkin, Y. E. Pronin, S. S. Vesely, L. P. Kazansky, Electrochemical and xps study of 2-mercaptobenzothiazole nanolayers on zinc and copper surface, Int. J. Corros. Scale Inhib. 3 (2) (2014) 78–88. doi:10.17675/2305-6894-2014-3-2-078-088.

[21] L. P. Kazansky, I. A. Selyaninov, Y. I. Kuznetsov, Adsorption of 2-mercaptobenzothiazole on copper surface from phosphate solutions, Appl. Surf. Sci. 258 (2012) 6807–6813. doi:10.1016/j.apsusc,2012.03.097.

[22] S.-J. Huo, L.-H. Chen, Q. Zuh, J.-H. Fand, Surface-enhanced infrared absorption spectroscopy study of anticorrosion behavior of 2-

mercaptobenzothiazole on copper, Acta Phys. -Chim. Sin. 29 (12) (2013) 2565–2572. doi:10.3866/PKU.WHXB201310294.

[23] M. Finšgar, D. K. Merl, An electrochemical, long-term immersion, and XPS study of 2-mercaptobenzothiazole as a copper corrosion inhibitor in chloride solution, Corros. Sci. 83 (2014) 164–175. doi:https://doi.org/10.1016/j.corsci.2014.02.016.
URL http://www.sciencedirect.com/science/article/pii/S0010938X14000754

[24] L. P. Kazansky, Y. E. Pronin, I. A. Arkhipushkin, XPS study of adsorption of 2-mercaptobenzothiazole on a brass surface, Corros. Sci. 89 (2014) 21–29. doi:10.1016/j.corsci.2014.07.055.

[25] M. Ohsawa, W. Suëtaka, Spectro-electrochemical studies of the corrosion inhibition of copper by mercaptobenzothiazole, Corros. Sci. 19 (10) (1979) 709 – 722. doi:http://dx.doi.org/10.1016/S0010-938X(79)80142-0.
URL http://www.sciencedirect.com/science/article/pii/S0010938X79801420

[26] H. M. Wilson, Near-infrared Fourier transform surface enhanced Raman scattering detection of mercaptobenzothiazole on smooth copper, Vib. Spectrosc. 7 (3) (1994) 287 – 291. doi:http://dx.doi.org/10.1016/0924-2031(94)85018-6.
URL http://www.sciencedirect.com/science/article/pii/0924203194850186

[27] J. Marconato, L. Bulhões, M. Temperini, A spectroelectrochemical study of the inhibition of the electrode process on copper by 2-mercaptobenzothiazole in ethanolic solutions, Electrochim. Acta 43 (7) (1998) 771 – 780. doi:http://dx.doi.org/10.1016/S0013-4686(97)00204-1.
URL http://www.sciencedirect.com/science/article/pii/S0013468697002041

[28] H. Nishizawa, O. Sugiura, Y. Matsumura, M. Kinoshita, Evaluation of mercaptobenzothiazole anticorrosive layer on Cu surface by spectroscopic ellipsometry, Jpn. J. Appl. Phys. 46 (2007) 2892–2894. doi:10.1143/JJAP.46.2892.

[29] J. Li, C. W. Du, Z. Y. Liu, X. G. Li, M. Liu, Inhibition film formed by 2-mercaptobenzothiazole on copper surface and its degradation mechanism in sodium chloride solution, Int. J. Electrochem. Sci. 11 (2016) 10690–10705. doi:10.20964/2016.12.46.

[30] R. Woods, G. A. Hope, K. Watling, A SERS spectroelectrochemical investigation of the interation of 2-mercaptobenzothiazole with copper, silver and gold surfaces, J. Appl. Electrochem. 30 (2000) 1209–1222. doi:10.1023/A:1026561914338.

[31] H.-F. Wang, Y.-G. Yan, S.-J. Huo, W.-B. Cai, Q.-J. Xu, M. Osawa, Seeded growth fabrication of Cu-on-Si electrodes for in situ ATR-SEIRAS applications, Electrochim. Acta 52 (19) (2007) 5950 – 5957. doi:http://dx.doi.org/10.1016/j.electacta.2007.03.042.
URL http://www.sciencedirect.com/science/article/pii/S0013468607004161

[32] S. Nayak, P. U. Biedermann, M. Stratmann, A. Erbe, In situ infrared spectroscopic investigation of intermediates in the electrochemical oxygen reduction on n-Ge(100) in alkaline perchlorate and chloride electrolyte, Electrochim. Acta 106 (2013) 472 – 482. doi:10.1016/j.electacta.2013.05.133.

[33] S. Nayak, P. U. Biedermann, M. Stratmann, A. Erbe, A mechanistic study of the electrochemical oxygen reduction on the model semiconductor n-Ge(100) by ATR-IR and DFT, Phys. Chem. Chem. Phys. 15 (2013) 5771–5781. doi:10.1039/C2CP43909C.
URL http://dx.doi.org/10.1039/C2CP43909C

[34] C. Toparli, A. Sarfraz, A. Erbe, A new look at oxide formation at the copper/electrolyte interface by in situ spectroscopies, Phys. Chem. Chem. Phys. 17 (2015) 31670–31679. doi:10.1039/C5CP05172J.
URL http://dx.doi.org/10.1039/C5CP05172J

[35] G. Genchev, A. Erbe, Raman spectroscopy of mackinawite FeS in anodic iron sulfide corrosion products, J. Electrochem. Soc. 163 (6) (2016) C333–C338. arXiv:http://jes.ecsdl.org/content/163/6/C333.full.pdf+html, doi:10.1149/2.1151606jes.
URL http://jes.ecsdl.org/content/163/6/C333.abstract

[36] Y. Chen, P. Schneider, A. Erbe, Investigation of native oxide growth on zinc in different atmospheres by spectroscopic ellipsometry, Phys. Status Solidi A 209 (2012) 846–853. doi:10.1002/pssa.201100542.

[37] Y. Chen, A. Erbe, In situ spectroscopic ellipsometry during electrochemical treatment of zinc in alkaline carbonate electrolyte, Surf. Sci. 607 (2013) 39 – 46. doi:10.1016/j.susc.2012.08.006.

[38] M. Hans, A. Erbe, S. Mathews, Y. Chen, M. Solioz, F. Mücklich, Role of copper oxides in contact killing of bacteria, Langmuir 29 (52) (2013) 16160–16166. arXiv:http://dx.doi.org/10.1021/la404091z, doi:10.1021/la404091z.
URL http://dx.doi.org/10.1021/la404091z

[39] ChemBK, http://www.chembk.com/en/chem/MBT (accessed 6 Nov. 2017).

[40] A. Altun, E. Kuliyev, N. M. Aghatabay, Tautomeric conversion, vibrational spectra, and density functional studies on peripheral sulfur derivatives of benzothiazole and benzothiazoline isomers, Spectrochim. Acta Mol. Biomol. Spectrosc. 152 (2016) 181 – 191. doi:http://dx.doi.org/10.1016/j.saa.2015.07.071.
URL http://www.sciencedirect.com/science/article/pii/S1386142515301207

[41] B. Cui, T. Chen, D. Wang, L.-J. Wan, In situ STM evidence for the adsorption geometry of three N-heteroaromatic thiols on Au(111), Langmuir 27 (12) (2011) 7614–7619, pMID: 21595454. arXiv:http://dx.doi.org/10.1021/la201155y, doi:10.1021/la201155y.
URL http://dx.doi.org/10.1021/la201155y

[42] M. K. Awad, M. R. Mustafa, M. M. Abouelnga, Quantum chemical studies and atomistic simulations of some inhibitors for the corrosion of Al surface, Prot. Met. Phys. Chem. 52 (1) (2016) 156–168. doi:10.1134/S2070205116010032.
URL https://doi.org/10.1134/S2070205116010032

[43] H. Y. H. Chan, C. G. Takoudis, M. J. Weaver, Oxide film formation and oxygen adsorption on copper in aqueous media as probed by surface-enhanced raman spectroscopy, J. Phys. Chem. B 103 (2) (1999) 357–365. arXiv:http://dx.doi.org/10.1021/jp983787c, doi:10.1021/jp983787c.
URL http://dx.doi.org/10.1021/jp983787c

[44] J. Kunze, V. Maurice, L. H. Klein, H.-H. Strehblow, P. Marcus, In situ STM study of the effect of chlorides on the initial stages of anodic oxidation of Cu(111) in alkaline solutions, Electrochim. Acta 48 (9) (2003) 1157 – 1167, microscopic and Nanoscopic Aspects of Corrosion and Corrosion Protection. doi:http://dx.doi.org/10.1016/S0013-4686(02)00826-5.
URL http://www.sciencedirect.com/science/article/pii/S0013468602008265

[45] B. K. Meyer, A. Polity, D. Reppin, M. Becker, P. Hering, P. J. Klar, T. Sander, C. Reindl, J. Benz, M. Eickhoff, C. Heiliger, M. Heinemann, J. Bläsing, A. Krost, S. Shokovets, C. Müller, C. Ronning, Binary copper oxide semiconductors: From materials towards devices, Phys. Status Solidi B 249 (8) (2012) 1487–1509. doi:10.1002/pssb.201248128.
URL http://dx.doi.org/10.1002/pssb.201248128

[46] L. Debbichi, M. C. Marco de Lucas, J. F. Pierson, P. Krüger, Vibrational properties of CuO and Cu_4O_3 from first-principles calculations, and Raman and infrared spectroscopy, J. Phys. Chem. C 116 (18) (2012) 10232–10237. arXiv:http://dx.doi.org/10.1021/jp303096m, doi:10.1021/jp303096m.
URL http://dx.doi.org/10.1021/jp303096m

[47] C. Toparli, A. Erbe, State of the surface of antibacterial copper in phosphate buffered saline, J. Electrochem. Soc. 164 (2017) H734–H742. doi:10.1149/2.0351712jes.